Journal of Applied Fluid Mechanics, Vol. 18, No. 2, pp. 399-418, 2025.
Available online at www.jafmonline.net, ISSN 1735-3572, EISSN 1735-3645.
https://doi.org/10.47176/jafm.18.2.2910

Intelligent Prediction of Separated Flow Dynamics using Machine Learning

S. Kouah[1,2†], F. Fadla[2,3] and M. Roudane[1]

[1] *Research laboratory of applied and fundamental physic /Blida 1 University BP 270 Route Soumâa, Blida, Algeria*
[2] *Research Laboratory of energetic, flow and transfers /AMC BP 48 Cherchell terre 42006, Tipaza, Algeria*
[3] *LAMIH, UMR-CNRS 8201, Department of Mechanical Engineering, University of Valenciennes and Hainaut-Cambresis, Valenciennes 59300, France*

†*Corresponding Author Email: kouah_salim@univ-blida.dz*

ABSTRACT

Understanding separated flow dynamics is crucial for implementing effective flow control techniques. These techniques help mitigate adverse effects on vehicle performance and environmental pollution. This research aims to improve flow control strategies by predicting separated flow dynamics solely through wall pressure measurements using artificial intelligence and numerical data. Initially, we identify numerical models that accurately replicate separated flow dynamics. Notably, the Detached Eddy Simulation (DES) model strongly agrees with experimental data, particularly in the turbulent regime at Re_h= 89100, downstream of backward facing steps (BFS). Subsequently we conducted a correlational analysis that revealed a significant relationship between various wall pressure points and the velocity field, leading to the adoption of deep learning techniques such as Recurrent Neural Networks with Long Short-Term Memory (LSTM). These neural networks, tailored for time-dependent data, demonstrate high accuracy of low MSE of 13.48% using ten wall pressure points in predicting velocity magnitude contour over (BFS). To enhance predictions, Proper Orthogonal Decomposition (POD) is utilized to reduce system complexity while retaining essential dynamics, resulting in a lower MSE of 5.07%. Additionally, we identify the ideal wall pressure measurement region that accurately captures the entire dynamic behavior, achieving an acceptable MSE of 23.48% for predicting low order vorticity, with only three wall pressure points. This research aids in developing efficient flow control strategies with limited pressure data and offers valuable insights for closed-loop flow control applications.

Article History

Received June 9, 2024
Revised August 18, 2024
Accepted September 5, 2024
Available online December 4, 2023

Keywords:

Flow separation
Backward facing step
Instabilities
LSTM Recurrent neural network
Dynamics prediction
Machine learning

1. INTRODUCTION

When an object is placed in a fluid flow, the fluid adheres to the surface of the body, but under certain conditions, it can detach from the wall, resulting in a phenomenon called flow separation. This is due to a positive pressure gradient or a geometric rupture of the wall, and it strongly affects the object's aerodynamic performance by increasing drag force and reducing lift in airplanes. Flow separation is a source of unsteadiness that can engender acoustic pollution and vibrations in the structure. Considering the deleterious impacts of this phenomenon, it is necessary to devise effective flow control techniques to ameliorate these effects. However, the successful implementation of such techniques necessitates a deep comprehension of the flow characteristics and the determination of the key parameters using advanced methods for achieving real time effective controls**.** In real-world applications, particularly in the design of intelligent flow control systems, we require dynamic information about the flow before applying control techniques such as synthetic jets. In practical scenarios, it is often not feasible to install sophisticated equipment to detect flow dynamics in real time. Instead, wall-mounted pressure sensors can be used to predict the velocity field. This approach is practical for real-time applications where rapid feedback is essential for effective flow control. This study's primary goal is to predict separated flow dynamics based on wall pressure measurements. Properly capturing and predicting flow separation is essential for optimizing closed-loop control strategies and enhancing the overall performance of aerodynamic systems. We worked extensively with numerical data. Before delving into this, it is essential to

NOMENCLATURE

AR	Aspect Ratio	X_r	internal reattachment length
ER	Expansion Ratio	L_r	external reattachment length
Re_h	Reynolds number	f	frequency
δ	jet diameter	$U_i(x,t)$	reconstructed field variable u at spatial location x and time t using the i^{th} mode.
u	longitudinal velocity	$a_n(t)$	time coefficients associated with each mode
v	normal velocity	$\Phi(x)_n^{(i)}$	i^{th} pod mode at spatial location x, with n modes in total.
p	pressure	ν	kinematic viscosity
ε	turbulent dissipation rate	L_t	turbulence length scale
ρ		t	time
C_{DES}	a constant used in DES models to control the transition between RANS and LES regions	Δ_{max}	largest spacing between grid points in the computational mesh
S_t	Strouhal number	ζ	vorticity magnitude

ensure the accuracy of our numerical data by validating it through experiments conducted under the same operating and geometrical conditions. Specifically, we focused on studying the flow over a (BFS) in a turbulent regime at Re_h=89100. The BFS is the most preferred geometry in academic and industrial studies of the separated flow for its simplicity, (Duriez et al., n.d.) and it offers adequate conditions to create the separation by geometric rupture by studding it with an angle of 90°. (Antonio & Lacerda De Brederode, n.d.) focused on the aspect ratio for BFS (AR=the wide of the test section/high step). They conclude that an aspect ratio greater than ten results in a two-dimensional flow, as the effect of side walls becomes negligible. Also, Ötügen (1991) studied the influence of the expansion ratio (ER = high of test section / (high of test section - high step)) on organized structures. Sujar Garrido et al. (2014) assured that BFS depends on two parameters: flow conditions (boundary layer, turbulence) and geometric ones (ER and AR). Chovet et al. (2017) worked on BFS with an effective nominal two-dimensional flow with an ER = 1.04 and AR = 24, resulting in negligible inference of the upper wall and side walls, and we conducted our research under the same conditions as (Chovet et al., 2017). And we assessed the DES model's accuracy in capturing turbulent flow dynamics, downstream of the BFS. After that, we conducted a correlative study involving ten (10) measurement points along both the vertical and horizontal walls of BFS. We explored the relationship between the wall pressure measurements and the velocity field in different components, in longitudinal (X) and normal (Y) directions. This correlation analysis helps us understand how pressure measurements correspond to the velocity field, a crucial aspect of our research. The next phase involves implementing a machine learning technique. In recent years, substantial advancements in deep learning techniques such as Ivakhnenko and Lapa (1965); Ivakhnenko (1971); Bengio (2009); Carrio et al. (2017); Khan and Yairi, (2018) have led to widespread adoption for information extraction across diverse data types. Various deep learning architectures have emerged. One prominent architectural is the recurrent neural network (RNN), as discussed by Robinson and Fallside (1987), Werbos (1988), Williams (1989), and Ranzato et al. (2014). The temporal challenges faced by Convolutional Neural Networks (CNN) and Deep Neural Networks (DNN) in handling sequential data like text, audio, and video, referencing studies by Fukushima (1980), LeCun et al. (1989), Weng et al. (1993), Rawat and Wang (2017), Guo et al. (2017), and Sharma and Singh (2017). In response to these challenges, (RNNs), particularly discrete-time RNNs, are emphasized for sequential data tasks. The distinctive cyclic connection in RNN architecture, enabling updates based on past and present data, is highlighted, referencing studies by Pearlmutter (1989), Brown et al. (2004), and Gallagher et al. (2005). Standard RNNs, including fully connected RNNs, Elman, (1990); Jordan, (1986); Chen and Soo (1996) and selective RNNs, Šter, (2013), are noted for their successes but acknowledged for struggling with long-term dependencies. To address this, Hochreiter and Schmidhuber's seminal worked in 1997 on Long Short-Term Memory (LSTM) networks is cited, emphasizing LSTM's significance in handling long-term dependencies in sequential data. It is a new type of RNN architecture that is widely used for sequential and time series data analysis. Unlike traditional RNNs, LSTM networks are specifically designed to capture long-term dependencies and handle the vanishing gradient problem. LSTMs have a unique memory cell that allows them to retain and selectively forget information over time. This memory cell is controlled by three main components: an input gate, a forget gate, and an output gate. These gates regulate the flow of information, enabling LSTMs to capture relevant patterns and ignore irrelevant or noisy input. LSTMs have found success in various tasks, including natural language processing, speech recognition, sentiment analysis, and time series forecasting. Their ability to model long-term dependencies make them particularly effective for tasks that involve capturing context and understanding sequences of data. which is the case of the unsteady flow dataset. Fernández et al. (2007), He and Droppo (2016), Hsu et al. (2016), Sak et al. (2014), Qu et al. (2017), Altché and Fortelle (2017), Palangi et al. (2015) and Mallinar and Rosset (2018) demonstrate and underline the success of the LSTM method in machine learning with data depending on time (Yu et al., 2019). In addition, (Kumar & Selvaraj, 2023) has compared the efficiency of LSTM model and the combination of this model with Black Widow Optimization Algorithm (BOA) and Mayfly

Optimization Algorithm (MOA) which has done a great result in accuracy. In the domain of fluid dynamics, the application of artificial intelligence (AI) methods and prediction has been explored in various research studies. For instance, the research by Fadla et al. (2016) investigates the use of electrochemical sensors for real-time stochastic reconstruction of large-scale dynamics in separated flows, focusing on accurately measuring wall shear stress to capture low-frequency flapping modes in transitional flow regimes at an inflow Reynolds number of 1735. By integrating electrochemical sensors with Particle Image Velocimetry (PIV) and utilizing (POD) and Linear Stochastic Estimation (LSE), the study creates a low-order model that effectively reduces flow separation by resolving low-frequency dynamics. However, the methodology faces challenges in high Reynolds number regimes due to potential measurement errors and complexities in capturing high-frequency dynamics. In another study, (Talele et al., 2021) use Computational Fluid Dynamics (CFD) and Artificial Neural Networks (ANN) to predict flow patterns around square and rectangular bluff bodies at higher Reynolds numbers, ranging from 63651 to 636505. This research demonstrates the capability of ANN, driven by CFD data, to accurately predict vortex generation and flow separation behavior, validated through a neuron independency study (CFD ANN rectangular), despite the high accuracy, the effectiveness of ANN is highly dependent on the quality and quantity of training data, and extensive computational resources are required for model training and validation. Further extending the application of ANN, (Rajabi & Kavianpour, 2012) developed a Levenberg-Marquardt (LM) neural network to predict turbulent flow over a BFS using Direct Numerical Simulation (DNS) data. The study highlights the efficiency of ANN in capturing complex flow dynamics and achieving high accuracy in flow prediction across different Reynolds regimes (ANN). Additionally, (Singh et al., 2017) applied ANN for predicting turbulent separated flows over airfoils, improving the accuracy of lift, surface pressure, and flow separation predictions across various Reynolds numbers. (ANNs) are generally effective for various types of data, including static data and data that depends on time. However, their effectiveness in handling time-dependent data can be limited compared to specialized neural network architectures designed for temporal sequences. The Focused Time-Delay Neural Networks (FTDNN) approach by (Giannopoulos & Aider, 2020) demonstrates that a shallow neural network architecture, when combined with POD, can achieve high accuracy in predicting flow dynamics. The study emphasizes the importance of time-delay in the inputs to capture temporal dependencies effectively. The optimal configuration included 501 neurons in the hidden layer and a time-delay of 400 steps, resulting in a validation mean squared error (MSE) lower than 10% for all POD coefficients, however, the necessity of selecting appropriate time-delay and network configuration parameters can complicate the model development. As a result, significant advancements have been made in the field of flow dynamics prediction using artificial neural networks (ANNs). Various studies have demonstrated the potential of ANNs in predicting flow behavior. However, these methods often face limitations when dealing with large datasets and time-dependent data. For instance, while ANNs can model complex patterns, their performance can degrade with increasing data size and temporal dependencies. Previous research has explored different methods to address these challenges. One such method is the (FTDNN) coupled with (POD), which helps in resolving temporal dependencies. However, this method poses a challenge in selecting the appropriate time delay, which can significantly affect the prediction accuracy. In this context, our study introduces the (LSTM) network, which is known for its efficiency in handling time-dependent data. LSTM networks have demonstrated superior performance in capturing temporal dynamics due to their memory capabilities. This makes them particularly suitable for applications involving large datasets with temporal dependencies, such as flow dynamics prediction. Despite its advantages, the LSTM approach may require substantial computational resources and a well-structured training dataset to achieve optimal performance. In this study we aim to create a model that can predict the velocity field based on the measured wall pressure, providing valuable insights into the flow behavior. Furthermore, we employ (POD) as a technique to reduce the complexity of the system while retaining the most significant dynamic information. This step simplifies the data and prepares it for a more efficient machine learning. Despite the progress in using neural network for flow prediction, there is a gap in leveraging the full potential of LSTM networks for this application. Our research aims to fill this gap by demonstrating the effectiveness of LSTM networks in predicting flow dynamics with high accuracy. The novelty of our approach lies in the integration of LSTM networks with POD to reduce system complexity while retaining essential dynamics. Additionally, we have conducted an investigation to find the best region based on three wall pressure measurements that can better predict the dynamics over a (BFS) and trained with reduced-order vorticity. We presented a comprehensive evaluation of the model's accuracy and efficiency, highlighting the potential of LSTM networks to improve flow control strategies. Achieving accurate vorticity predictions with limited data (wall pressure measurements) could be instrumental in implementing closed-loop control systems with limited pressure measurements, and it is a valuable technique for scientists and engineers who work in this field and are involved in developing flow control systems.

2. NUMERICAL MODELING

2.1 Hypotheses

Before conducting any numerical simulation, it's essential to formulate our hypothesis, which serves as the foundation for our research to draw meaningful conclusions. As we are working on the same operating conditions as (Chovet et al., 2017) (experimental), we suppose that:

- Two-dimensional flow (when the aspect ratio greater than ten (Antonio & Lacerda De Brederode, n.d.) the flow is predominantly two-dimensional, and the transversal dynamics become negligible, effectively

the effects of the side walls is minimized). In addition, our study aims to establish a closed-loop control system capable of predicting and managing the most significant flow dynamics. To achieve this, we focused on the longitudinal and normal dynamics where the most critical flow behaviors are observed in experiments. Consequently, we opted for two-dimensional simulations, as the transversal dynamics are less significant in our case.

- Walls are adiabatic.
- Fluid is air with (density (kg/m^3) =1.225 and dynamic viscosity (kg/ m s) = 1.7894.10^{-5}).
- Incompressible flow.
- Isothermal flow (experimental work was done in fixed temperature).
- Turbulent flow at (Re_h = 89100) and (Re_h = 31500 for comparing with experimental wall pressure coefficients).
- Turbulent intensity equals 0.6% (same measured in experimental conditions).
- Thickness of boundary measured at 0.2 h before BFS, δ/h = 0.5060 (as measured in experimental work, showing equivalent values at the same location).

2.2 Simulation Domain

We conducted our simulation using the same geometrical and operating conditions, as those employed in the experiments at (Chovet et al., 2019), we worked with the height step value, h = 0.083 m, as shown in Fig. 1-a and Fig. 1-b.

2.3 Meshing

In our case, the geometry is not complex, and we did not hesitate to choose the structured mesh for our study. In 2D, the elements are quadrilaterals as shown in Fig. 1-b, and it presents the following advantages:

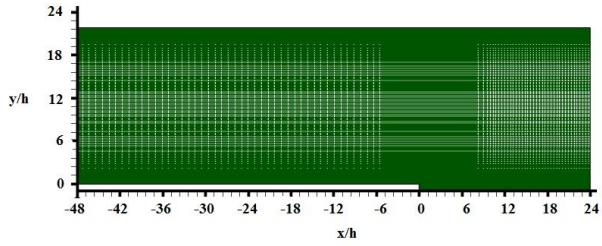

Fig. 1-a Computational Domain with Coordinates

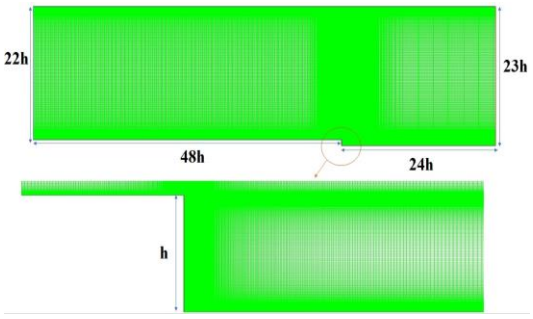

Fig. 1-b Visualization of Mesh within the Computational Domain

- Economic in number of elements, it presents a lower number of cells than an equivalent unstructured mesh.

- When the mean flow is aligned with the mesh, a structured mesh reduces the risk of numerical errors.

We refined the mesh near both the vertical and horizontal walls. This type of meshing is largely used in the literature for (BFS) as well as for vertical and horizontal walls, such as squares like the meshing over two inline square cylinders (Sohankar et al., 2019). To accurately capture the boundary layer, we implemented the y^+ approach to achieve an appropriate wall resolution, targeting a value of y^+=1 to ensure that the mesh resolves the viscous sublayer in all cases. Additionally, all meshes were generated by varying the cell-to-cell growth ratio as shown in Fig. 2-a at the BFS corner.

The choice of mesh size is crucial to balancing accuracy and computational efficiency. Therefore, we conducted a sensitivity analysis to determine the optimal mesh size for our simulations. We assessed the mesh quality using various criteria, including skewness, aspect ratio, and orthogonality. We achieved a high-quality mesh with smooth transitions between the different zones, ensuring accurate numerical predictions of the flow dynamics over the BFS. In the Fig. 2-b, the plot shows how the viscous coefficient changes with the number of nodes used in the meshing. Initially, the viscous coefficient fluctuates significantly as the number of nodes increases, indicating a lack of convergence. At around 580,000 nodes, the viscous coefficient stabilizes and shows minimal variation with further increases in the number of nodes. Indicating that the solution has reached a converged state where further refinement does not significantly affect the results. Figure 2-c, illustrates the wall shear stress downstream of BFS plotted against x/h for various mesh resolutions. It offers insights into the internal and external reattachment lengths, with reattachment points identified by values approaching zero, indicating where the flow reattaches after separation. The dashed lines indicate experimental values for x/h=0.71 (X_r in exp) and x/h=5.37 (L_r in exp). As the mesh resolution increases, the curves converge, becoming closer to the experimental values. The meshes with more than 550000

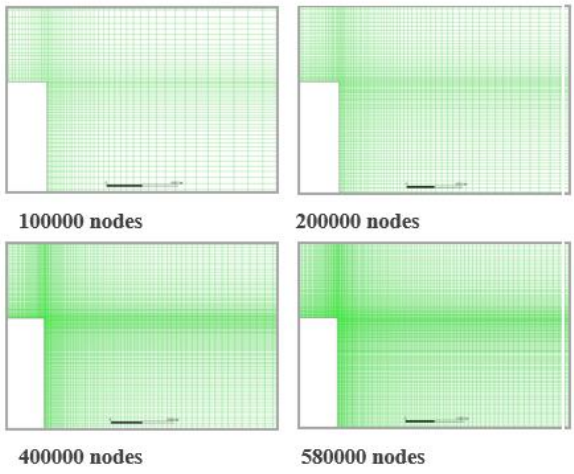

Fig. 2-a Examples of Analyzed Meshes

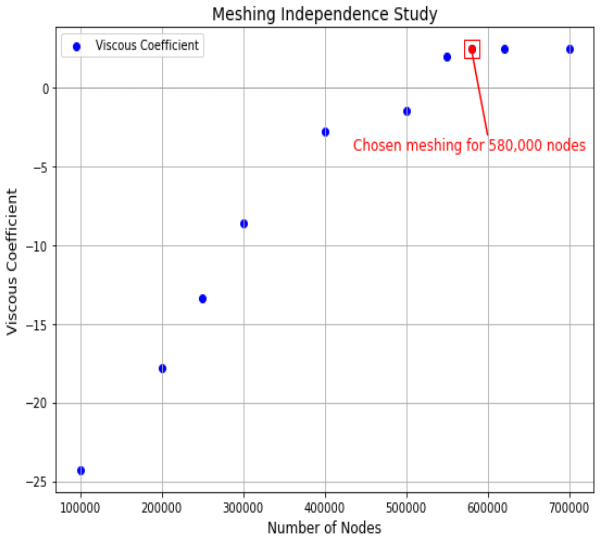

Fig. 2-b Meshing Independence study using viscous coefficient

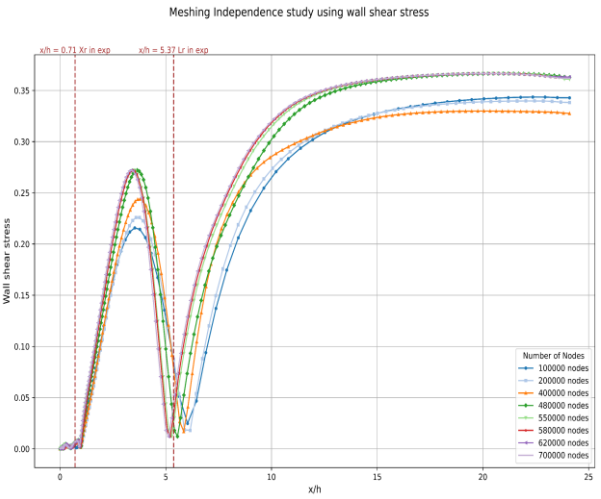

Fig. 2-c Meshing Independence study using wall shear stress

nodes are particularly well-aligned and closely match the experimental values at both X_r and L_r. Consequently, selecting 580000 nodes offers a good balance between computational cost and accuracy, as this choice is informed by the stabilization of both the viscous coefficient and the convergence of wall shear stress values, making it the optimal mesh resolution for this study.

2.4 Numerical Models

To perform simulations in our study, we used Ansys Fluent due to its versatility and wide range of available numerical models, with finite volume discretization, and the momentum equations were solved using the MUSCL third-order scheme, while the other equations were solved using second-order schemes. Additionally, residual values were set to 10^{-6} for better precision, ensuring higher accuracy in the numerical solutions. In the context of 2D unsteady isothermal flow, the governing equations consist of the continuity equation for mass conservation and the momentum equations. The continuity equation ensures that mass is conserved in the flow, and it can be expressed as:

Continuity Equation (Mass Conservation)

$$\frac{\partial u}{\partial x}+\frac{\partial v}{\partial y}=0 \tag{1}$$

The momentum equations, which describe the forces acting on the fluid, are essential for capturing the dynamics of the flow.

Momentum Equations

x-momentum Equation

$$\frac{\partial u}{\partial t}+u\frac{\partial u}{\partial x}+v\frac{\partial u}{\partial y}=-\frac{1}{\rho}\frac{\partial p}{\partial x}+\nu\left(\frac{\partial u^2}{\partial x^2}+\frac{\partial u^2}{\partial y^2}\right) \tag{2}$$

y-momentum Equation

$$\frac{\partial v}{\partial t}+u\frac{\partial v}{\partial x}+v\frac{\partial v}{\partial y}=-\frac{1}{\rho}\frac{\partial p}{\partial y}+\nu\left(\frac{\partial v^2}{\partial x^2}+\frac{\partial v^2}{\partial y^2}\right) \tag{3}$$

Choosing the appropriate turbulence model is especially important, as turbulence plays a crucial role in many fluid flows. However, selecting a more complex model may not always lead to better results, as it may require more computational resources and time. Overall, a systematic approach that considers the physical phenomena being studied, and the available computational resources is necessary to select an adequate numerical model. Several researchers have investigated different turbulence models to reproduce the important flow features on BFS, observed in the experiments. Šarić et al. (2005) conducted a study on Large Eddy Simulation (LES), Detached Eddy Simulation (DES), and the Reynolds Stress Model (RSM). They concluded that while LES and DES are the most accurate, RSM also has positive aspects, particularly in handling complex three-dimensional flows and capturing anisotropic turbulence effects. Also (Mehrez et al., 2010) has used LES model to show the influence of a periodic perturbation on BFS. (Luo, 2019) found that partially averaged Navier-Stokes (PANS) gives acceptable predictions in BFS but is less accurate than the DES model. Additionally, the study by (Probst et al., 2010) on separation behind the BFS showed that DES variants agree well with measured skin friction and velocity profiles when a sufficiently fine mesh is applied, unlike RSM. Almohammadi (2020) found that the Transition-SST model effectively captures the laminar-turbulent transition, providing accurate predictions in flow separation scenarios. (Smirnov et al., 2018) concluded that the Improved Delayed Detached Eddy Simulation (IDDES) model offers significant improvements over traditional DES and RANS models, particularly in predicting heat transfer and reattachment lengths in BFS flows. Other models designed to include laminar-turbulent transition and separation, such as Gamma-Reynolds and RMS, also offer significant potential for accurately predicting flow characteristics in BFS scenarios. These models account for the transition between laminar and turbulent flow, providing more comprehensive results in certain conditions. These findings demonstrate the importance of selecting an appropriate turbulence model based on the flow characteristics and objectives of the simulation.

DES (Detached Eddy Simulation)

DES is a hybrid turbulence model that combines the benefits of Reynolds-Averaged Navier-Stokes (RANS) and Large Eddy Simulation (LES) models. The DES model uses RANS equations in the near-wall regions and switches to LES equations in the outer regions, by a comparison of the turbulent length scale L_t with the grid spacing Δ_{max}. The model selects the minimum of both and switches between RANS and LES mode by replacing $\boldsymbol{\varepsilon}$ in the *k*-equation by:

$$\boldsymbol{\varepsilon} = \frac{\boldsymbol{k^{3/2}}}{\boldsymbol{L_t}} \rightarrow \quad \boldsymbol{\varepsilon} = \frac{\boldsymbol{k^{3/2}}}{\boldsymbol{min(C_{DES}\Delta_{max}, L_t)}} \tag{4}$$

The modified equation ensures a smooth transition between the RANS and LES regions in hybrid turbulence models. In regions where the grid is fine, the LES approach dominates, while in coarser grid regions, the RANS approach is used. This allows for better prediction of both attached and separated flows, making it a popular choice for simulating complex flow phenomena. The DES model involves solving a modified set of Navier-Stokes equations, which account for the effects of turbulence on the flow.

2.5 Proper Orthogonal Decomposition Technique

Proper Orthogonal Decomposition (POD) is a powerful technique used for analyzing and reducing the dimensionality of data. commonly applied in the field of fluid dynamics, and analyzing turbulent flows. The primary goal of POD is to extract the dominant coherent structures or modes from a given dataset. It decomposes the data into a set of orthogonal modes, which capture the major energy-containing structures in the flow. These modes are arranged in order of their significance, with the first mode representing the most energetic structure, followed by subsequent modes representing progressively less energetic structures. POD allows the representation of complex flow fields with a reduced number of modes. Modes are obtained by the function Φ(x) that has the largest mean square projection of u(x, t). The integral equation has a discrete set of solutions Φ(x) and n where n is the mode order of the orthogonal decomposition. The eigenfunction were orthonormal e.g. $\Phi(x)_n$, $\Phi(x)_p = \lambda_{np}$. Then the fluctuating velocity field can be decomposed as follow:

$$\boldsymbol{u_{i(x,t)} = \sum_{i=1}^{n_m} a_n\,(t)\Phi(x)_n^{(i)}(x),\ \ i = 1, \ldots, n} \tag{5}$$

2.6 Numerical Modeling Results

2.6.1 Flow Topology

The results using DES model at Re_h =89100 from the simulation are in good agreement with the experimental data (EXP), in the external reattachment length (L_r), internal separation length (X_r) as presented in Table 1.

Figure 3 presents the contours of mean flow velocities. In Fig. 3-a, the X velocity contours show that BFS creates a recirculation zone downstream of the step, which is characterized by negative velocities. However, after the reattachment point, a new boundary layer forms, and the velocity becomes positive again, indicating the recovery of the flow. These negative velocities in the recirculation zone and subsequent recovery of the flow are common features. Observed in the flow past a BFS.

Table 1 Comparison between experimental and numerical reattachment length

Models / Results	EXP	DES mean values
L_r/h	5.37	5.2870
X_r/h	0.71	0.6820
δ/h	0.53	0.5010

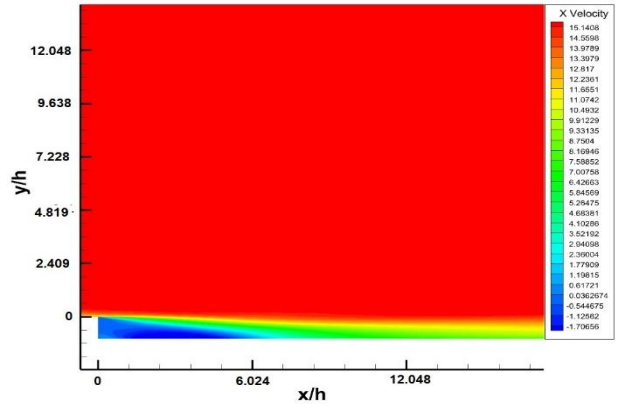

Fig. 3-a Contour of longitudinal velocity

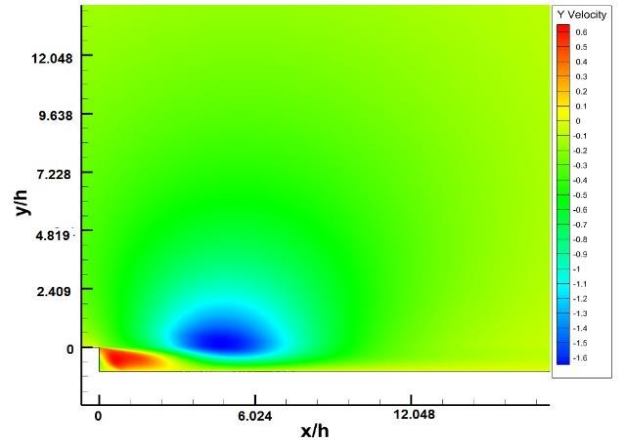

Fig. 3-b Contour of normal velocity
Fig. 3 Contours of mean flow velocities

Also, in Fig. 3-b (Y velocity), we saw that after sudden expansion followed by a sudden contraction, which can induce separation and the formation of a recirculation zone downstream of the step. The negative normal velocity is observed in this recirculation zone, this causes a separation of the boundary layer and the formation of a shear layer at the edge of the step. This shear layer is susceptible to various types of instabilities, such as vortex shedding, and vortices. In unsteady flows past a BFS, the dynamics of the shear layer and the formation of vortices and the shear layer oscillation can be observed and deform over time due to the unsteadiness of the flow, which can be seen as fluctuations in the velocity vectors. The formation and shedding of vortices can also be seen. These vortices can interact with each other and with the walls of the channel, leading to the formation of a recirculation zone downstream of the step.

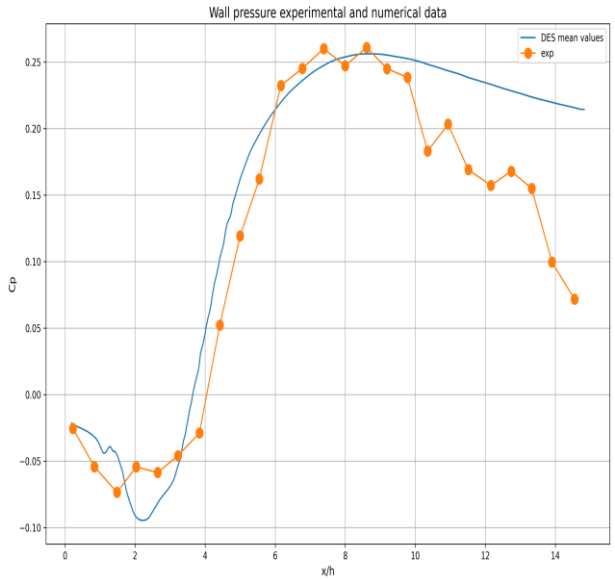

Fig. 4 Wall pressure coefficient investigated in Re_h = 31500 after BFS x/h =0-15 (experiments (Chovet et al., 2019) and numerical results (mean values for DES model)

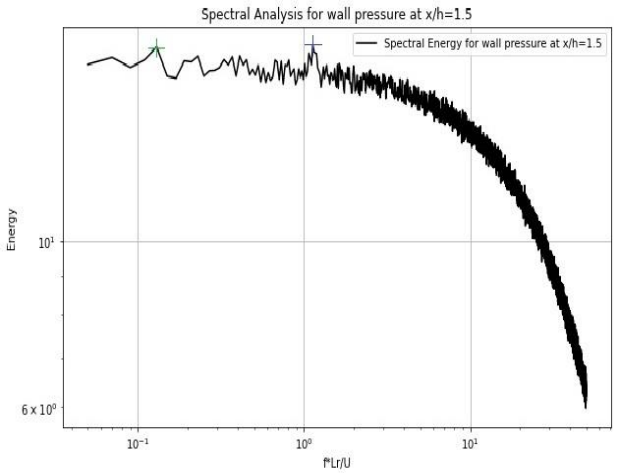

Fig. 5 Non-dimensional power spectra of fluctuating wall pressure measured at x/h=1.5 for our current study at Re_h = 89100

Wall Pressure Coefficient

The coefficient of pressure is the most essential parameter in our study, it highlights the mean flow topology, we compared our results of wall coefficient pressure after BFS with the experimental results measured by (20) pressure sensor Kulite XCQ – 062 by Chovet et al. (2019) at Re_h = 31500, shown in Fig. 4, a low-pressure level was seen for both results, a zero value of Cp is in x/h ≈ 4 for the experiment and near 3.5 for the DES model's mean values, with a maximum value of C_p near to 0.25 was for both results, after the external reattachment length equals 5.62, the pressure gradient becomes adverse as the expansion of the flow. The DES model effectively captures the overall trend and qualitative behavior of the flow, demonstrating its ability to detect depression and the relationship between wall dynamics and flow characteristics. The strong qualitative agreement between numerical and experimental results suggests that the model accurately represents the essential physics of the flow.

2.6.2 Spectral Analysis

Performing a spectral analysis quantifies instabilities and periodic phenomena, providing insights into the dynamic behavior of structures, vortices, and the separation bubble. This technique involves examining the frequency content of the flow field to identify the dominant frequencies and amplitudes of unsteady phenomena, characterizing their temporal and spatial features. The resulting data is valuable for identifying sources of unsteadiness and understanding the underlying flow dynamics. the best region to show the low-pressure fluctuations where the dynamic is dominated by both low and high frequencies is at $x/L_r < 0.3$ or exactly in x/h = 1.5, under the shear layer, and we evaluated the wall pressure in this region. Our spectral analysis results presented in Fig. 5 indicates the presence of two distinct instabilities in the flow past the studied object.

The first instability, visible as peak marked with green cross in the plot, is characterized by a low Strouhal number ($S_t = (f * L_r)/U_\infty \approx 0.12$) and corresponds to the flapping instability (oscillation of the shear layer). This instability is in agreement with previous studies reported in the literature by Chovet et al. (2019) and (Fadla et al., 2019). The second instability, shown as a little accumulation of energy marked with blue cross in the plot, has a higher Strouhal number ($S_t \approx 1$) and is associated with the formation and shedding of vortices, as reported in the literature by Chovet et al. (2019) and Fadla et al. (2019.). Our results are in excellent agreement with these previous studies.

3. MACHINE LEARNING AND PREDICTION

In this part, we have selected a rectangular area (Fig. 6) that includes the important zone containing the recirculation zone and the shear layer, which is crucial for our research, because they greatly affect how the flow behaves and the overall characteristics of the BFS. By focusing on these specific areas, we hope to better understand the complex dynamics and fundamental mechanisms of the phenomenon of separation flow. We have chosen a specific zone within the BFS. This zone spans from (x/h = 0) to (x/h = 9, 6385) along the x-axis and from (y/h = –1) to (y/h = 1.2048) along the y-axis. To analyze this zone effectively, we have created a mesh with 1600 elements, forming a matrix of dimensions (80,20), to discretize and represent the flow fields. accurately within the selected zone, enabling us to conduct detailed investigations and gather valuable data for our research. We have selected multiple points (Fig. 7) along the wall to measure the wall pressure. We can accurately capture and analyze the variations in wall pressure along the surface (vertical and horizontal wall around the recirculation zone), by strategically choosing these locations, to show the interaction and relationship between wall pressure and the separated flow on BFS dynamics.

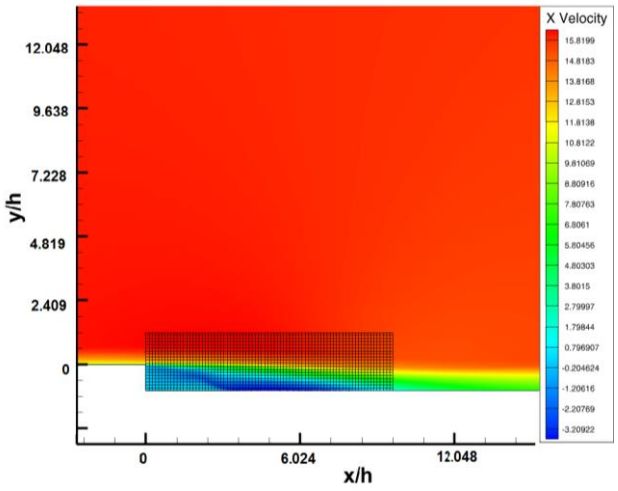

Fig.6 Chosen rectangular zone with mesh for study

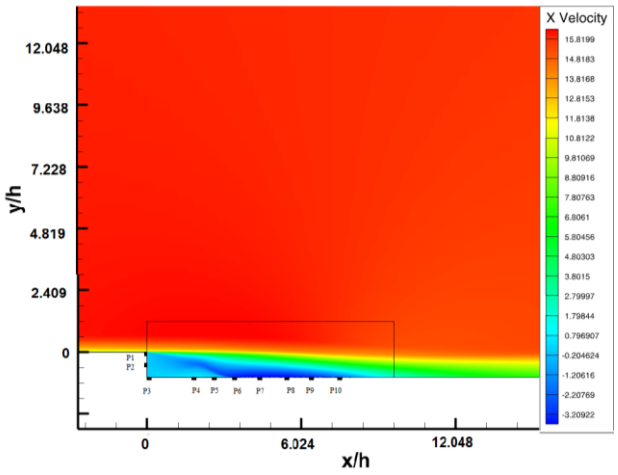

Fig. 7 Chosen ten points wall pressure for study

3.1 Corelative Study Between Wall Pressure and Velocity Field

Before diving into machine learning analysis between wall pressure and velocity field, it is essential to conduct a correlation study and examine the relationship between the variables involved and determine if there is a linear association between them. This preliminary investigation allows us to understand the degree of dependency between the variables, by assessing the strength and direction of the relationship. This correlation analysis is a crucial step before moving to machine learning, as it assesses the feasibility of the learning process by identifying significant features and relationships within the variables. We conducted individual correlation studies between each point of wall pressure and the corresponding velocity fields (X-velocity and Y-velocity). This analysis was performed for all points of wall pressure along the surface, by examining the correlation between a specific pressure point and the velocity field. We repeated this process for each point of wall pressure, allowing us to understand how changes in pressure relate to variations in the X-velocity and Y-velocity throughout the entire dataset. Using Python programming and its libraries to perform a correlation analysis between wall pressure and velocity. Initially, we imported necessary libraries such as numpy and pandas to handle data processing. We load the wall pressure data as a vector from a file and loaded the velocity data and coordinates from multiple files. Using the pandas library, for each coordinate point, we calculated the correlation between the pressure vector and the velocity components. The correlation coefficient, ranging from 0 to 1, indicates the strength of the relationship. These results were then written to an output file, which enabled us to create a contour plot visualizing the correlation strength at each point. This visualization illustrates how velocity at various points relates to wall pressure, providing valuable insights into the flow dynamics and ensuring that the machine learning model is trained on the most relevant and influential data. In Fig. 8, which represents the correlation with the X-velocity, along the horizontal walls, a positive correlation is observed near all pressure points, while a negative correlation is observed above these points. Regarding the vertical walls, specific locations exhibit distinct correlation characteristics. At Point 1, located at the summit of the BFS, a positive correlation is prominent. However, at Point 2, the correlation with the velocity field is weak. At Point 3, positioned at the corner, there is a moderate positive and negative correlation, apparent across all velocity fields. Furthermore, Fig. 9 shows correlations with Y velocity on the horizontal wall, points are in positive correlation with zone above after and negative correlation in zone before, and zones of strong correlation are near the wall in correlation with the points after the recirculation zone, and correlation with vertical wall pressure is weaker than horizontal wall, in addition we can observe that points under the shear layer (point 4 ,point 5 point 6 and point 7) have the strongest correlation with both X and Y velocity.

3.2 Methodology of Machine Learning Using LSTM NN Algorithm

3.2.1 LSTM Key Concepts

Memory Cell

The core element of an LSTM is the memory cell, which maintains information over time. It acts as a conveyor belt, passing along relevant information and selectively forgetting unnecessary information.

Gates

LSTMs utilize three types of gates to control the flow of information within the memory cell.

Cell State

The memory cell maintains the cell state, which carries information over time. The input gate and forget gate determine which information is added and forgotten, respectively, in the cell state.

Hidden State

The hidden state is the output of the LSTM at a given time step. It is derived from the cell state and passes through the output gate to produce the final output. During training, the LSTM adjusts its internal parameters using backpropagation through time (BPTT) to minimize the error between predicted and actual outputs. This process enables the network to learn and capture complex

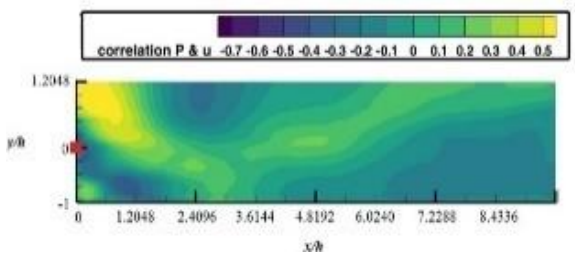

(a) correlation between u and P1

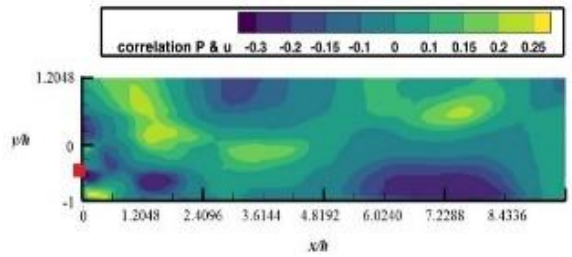

(b) correlation between u and P2

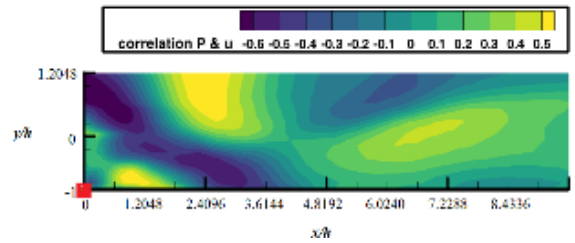

(c) correlation between u and P3

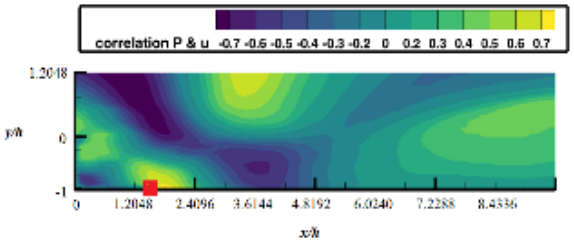

(d) correlation between u and P4

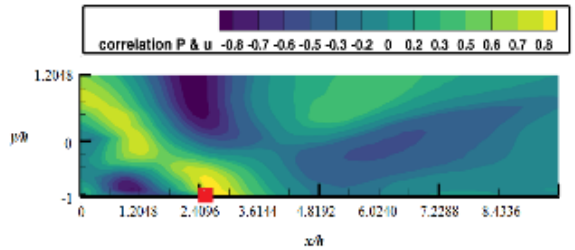

(e) correlation between u and P5

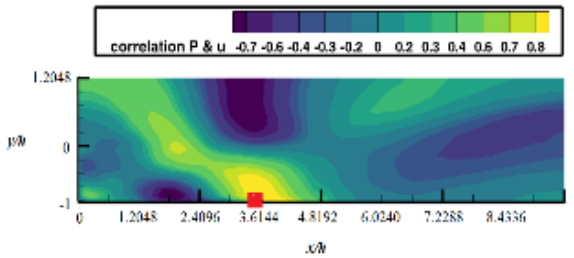

(f) correlation between u and P6

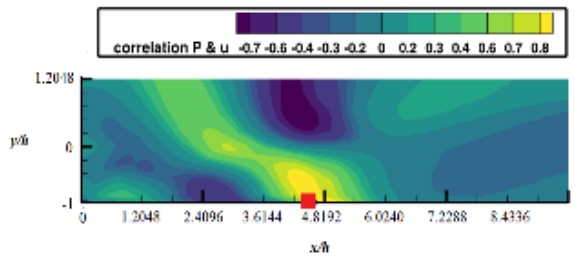

(g) correlation between u and P7

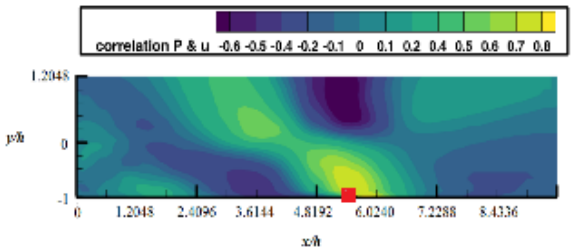

(h) correlation between u and P8

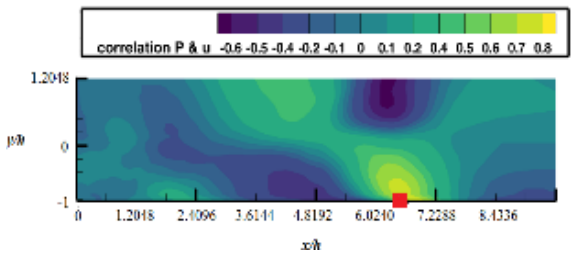

(i) correlation between u and P9

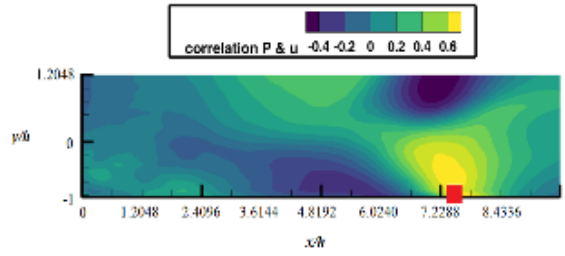

(j) correlation between u and P10

Fig. 8 correlation between u and wall pressure points

temporal patterns within sequential data. By leveraging the memory cell and gating mechanisms, LSTMs can effectively handle long-term dependencies, mitigate the vanishing problem.

These key concepts encapsulate the fundamental aspects of LSTMs and their mechanisms for processing sequential data.

3.2.2 Structure of the LSTM Model

The LSTM model used in our study is structured as follows:

Input Layer: Receives wall pressure data points as input extracted as time-dependent data.

LSTM Layer: Captures temporal dependencies in the data.

Dense Layers: Fully connected layers that transform the LSTM outputs into the desired format.

Output Layer: Produces the predicted velocity field corresponding to the input wall pressure measurements.

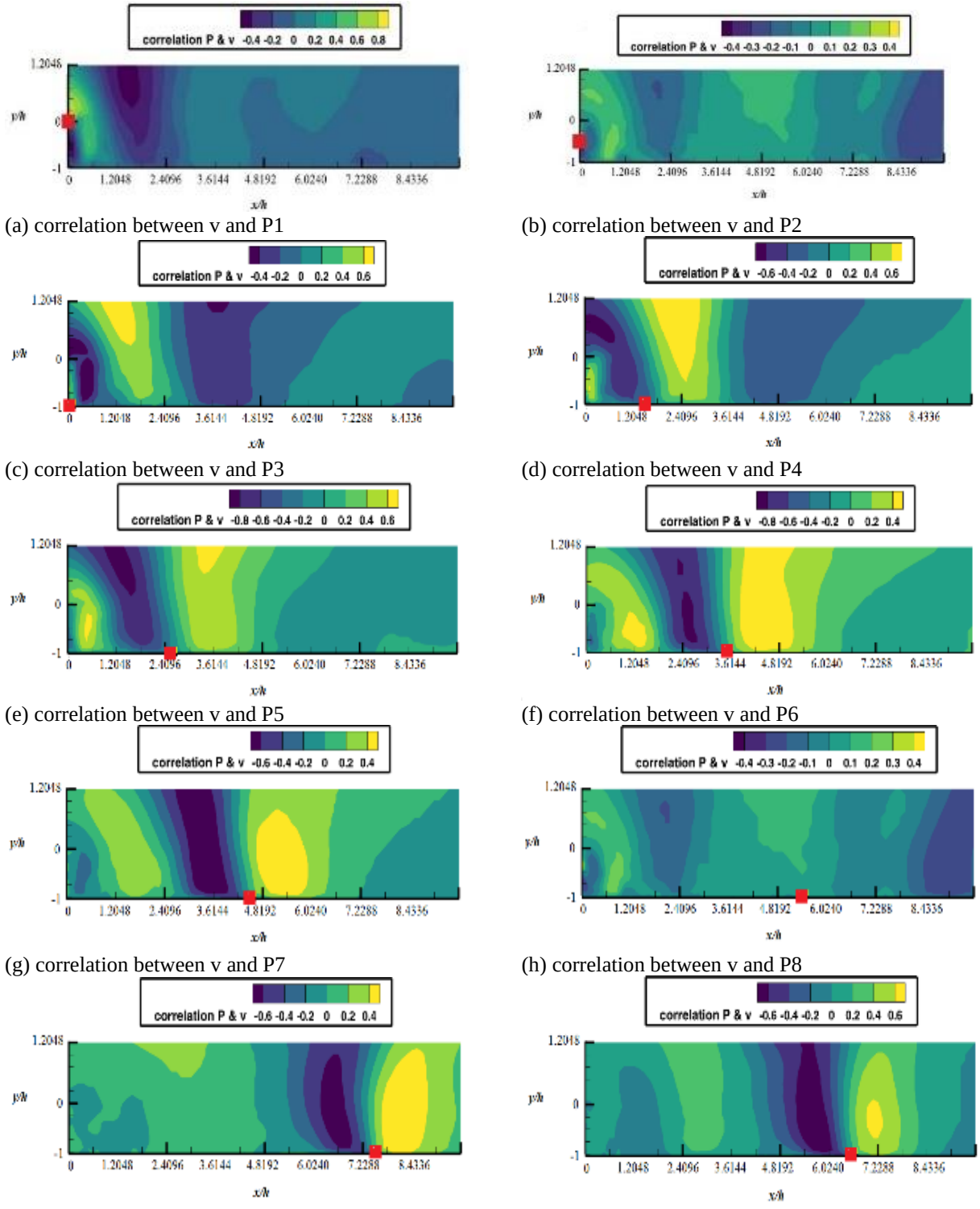

(a) correlation between v and P1

(b) correlation between v and P2

(c) correlation between v and P3

(d) correlation between v and P4

(e) correlation between v and P5

(f) correlation between v and P6

(g) correlation between v and P7

(h) correlation between v and P8

(i) correlation between v and P9

(j) correlation between v and P10

Fig. 9 correlation between v and wall pressure points

3.2.3 Machine Learning Process

- Load the pressure and velocity data in PYTHON, from the specified paths.
- Reshape and preprocess the data to prepare it for input into the LSTM network. This includes reshaping the pressure data to match the expected input shape of the LSTM and performing standard scaling on both the pressure and velocity data.
- Build the LSTM model using the Sequential API of TensorFlow's Keras. The model consists of LSTM layers followed by densely connected layers with various activation functions.
- Compile the model by specifying the loss function ('mean squared error') and optimizer ('adam').
- Define early stopping criteria to monitor the validation loss and stop training if the loss doesn't improve after a certain number of epochs.

- Train the model on the input data and target output, using the "fit" function. The training data is split into training (80%) of dataset and validation sets (20%) of dataset, and the early stopping criteria are applied.
- Evaluate the trained model on the test set using the "evaluate" function.
- Save the trained model to a file.
- Predict the output on the test set and calculate the mean squared error (MSE) between the predicted and actual values.
- Plot the training and validation loss over the epochs using matplotlib library.

3.2.4 Prediction Process

In the prediction phase, the saved model is loaded, and new input vectors (wall pressure) are provided. The trained model, which contains the coefficients, equations, and memories of the LSTM model, processes these inputs and generates the corresponding output matrices representing the velocity field. Here is a brief overview of the prediction process:

1-Load the Saved Model: The trained LSTM model is loaded from the saved .h5 file.

2-Load and Preprocess Pressure Data: New wall pressure data is loaded and preprocessed as required.

3-Predict Velocity Field: The model uses the input pressure data to predict the velocity field.

4-Save Predicted Data: The predicted velocity fields are saved to files for further analysis.

3.2.5 Hyperparameters Used in the Neural Network

We employed several hyperparameters to optimize the performance of our LSTM neural network:

Learning Rate: Controlled by the Adam optimizer, which adaptively adjusts the learning rate during training to ensure efficient convergence.

Number of Layers and Neurons: The model includes one LSTM layer with 16 units, followed by four dense layers with 32, 128, 512, and 1600 units, respectively. This configuration was chosen to balance model complexity and performance.

Batch Size: Set to 32, which determines the number of samples processed before the model's internal parameters are updated.

Epochs: Set to 1000, defining the number of complete passes through the training dataset. Early stopping was implemented to prevent overfitting, halting training when validation loss ceased to improve.

Activation Function: The ReLU (Rectified Linear Unit) activation function was applied to the dense layers, enabling the model to learn complex, non-linear relationships in the data by allowing for a broader range of outputs.

4. RESULTS AND DISCUSSION

4.1 Training Velocity Magnitude with Ten Points of Wall Pressure

Fig. 10 illustrates the workflow of a machine learning model that uses wall pressure data to predict velocity magnitude. The process begins with the collection of wall pressure measurements at ten (10) points. These measurements, along with corresponding velocity magnitude data, are used to train a (LSTM) (NN). Once trained, the model can predict the velocity magnitude using only the wall pressure points as input. The diagram effectively demonstrates the input-output relationship and the role of the machine learning model in transforming wall pressure data into meaningful velocity predictions. Training a model consisting of 3000 datasets has given promising results. The training process resulted in a minimal loss of 5.10%, showcasing the model's ability to effectively learn from the provided data. Furthermore, during the validation phase, the model demonstrated a slightly higher loss of 8.48%, as shown in Fig. 11, which remains within acceptable limits. Also, when applied to predict instantaneous snapshots, of velocities, the model exhibited accurate predictions, successfully preserving the correct topology of the contours as demonstrated in Fig. 12, the MSE is estimated to 13,486%, to be within acceptable values. Although there is a small difference in the actual velocity values, the overall topology remains accurate. The positions of shedding and vortex formations are correctly predicted, which is critical for our objective. Achieving higher precision would require a substantial amount of data and more powerful computational resources. These outcomes suggest that the trained model is robust and capable of capturing the underlying patterns within the data.

In Fig. 13, spectral analyses were conducted for both the original velocity data and the predicted normal velocity. Remarkably, the spectral plots exhibit striking

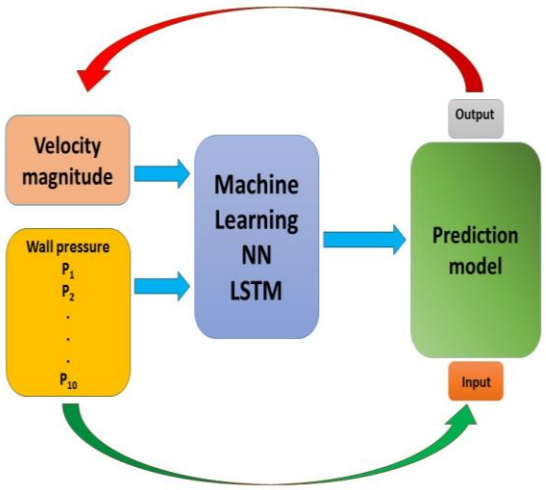

Fig. 10 Machine learning model with velocity field and ten wall pressure points

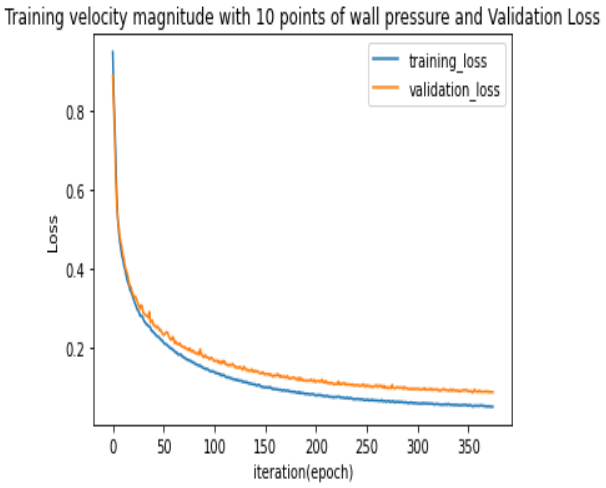

Fig. 11 Training velocity magnitude with 10 points of wall pressure

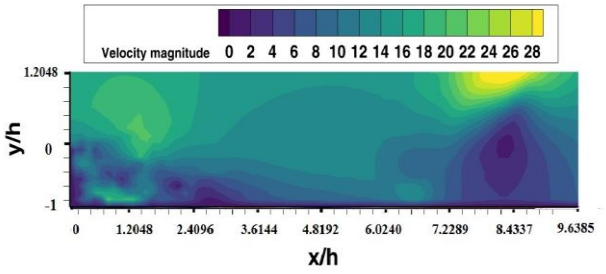

(a) Original velocity magnitude contour at t instant

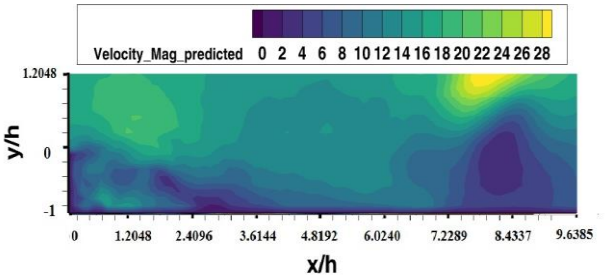

(b) Predicted velocity magnitude contour at t instant

Fig. 12 Predicting velocity magnitude contour with ten points of wall pressure at same instant

similarities, particularly in the peaks (the Strouhal number adjacent to 1 and at low frequencies 0.1). This quantitative agreement underscores the reliability of our predictions, providing strong confirmation of the presence of instabilities in both the original and predicted datasets.

4.2 Training Reduced Order Velocity Field with Wall Pressure

After applying the (POD) method to our dataset, a notable observation emerged: Mode 1 stands out as the most energetically significant, a finding visually depicted in the associated histogram in Fig. 14. The cumulative plot (Fig. 15) further reinforces this insight, illustrating that the sum of all decompositions (modes) collectively accounts for 100% of the energy.

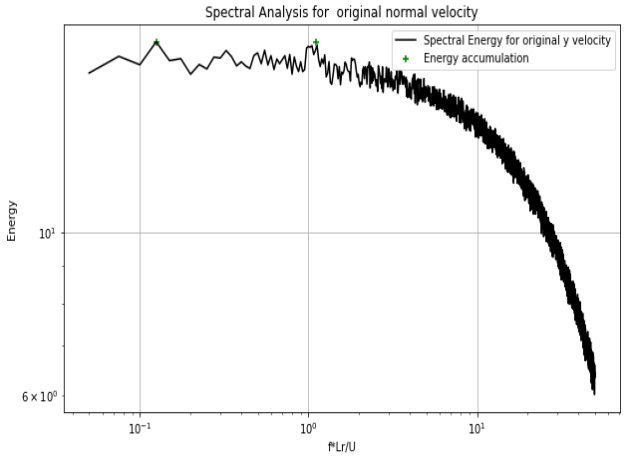

(a) Non-dimensional power spectra of fluctuating normal original velocity measured at x/h=1.5 at Re_h = 89100.

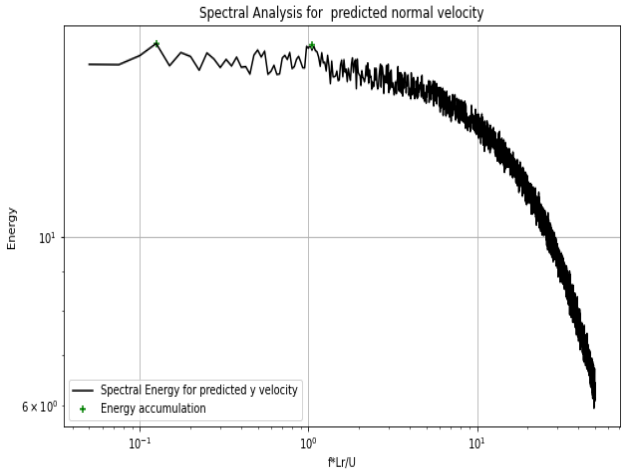

(b) Non-dimensional power spectra of fluctuating normal predicted velocity measured at x/h=1.5 at Re_h = 89100.

Fig. 13 Non-dimensional power spectra of fluctuating for original and predicted normal velocity measured at x/h=1.5 at Re_h = 89100

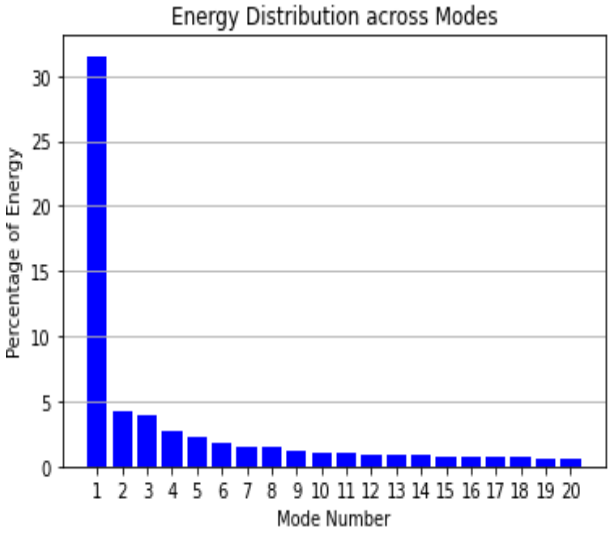

Fig. 14 Histogram shows the percentage of energy for each mode

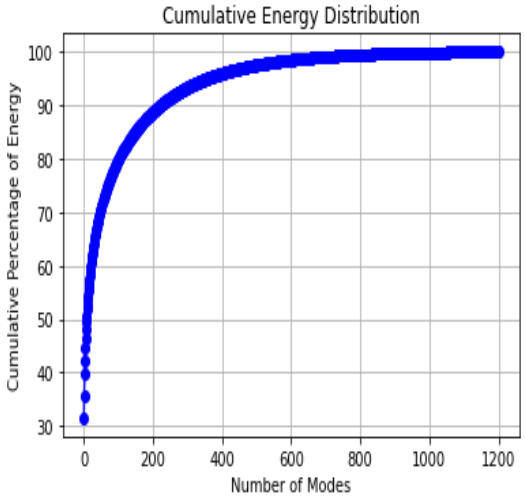

Fig. 15 Cumulative percentage of energy

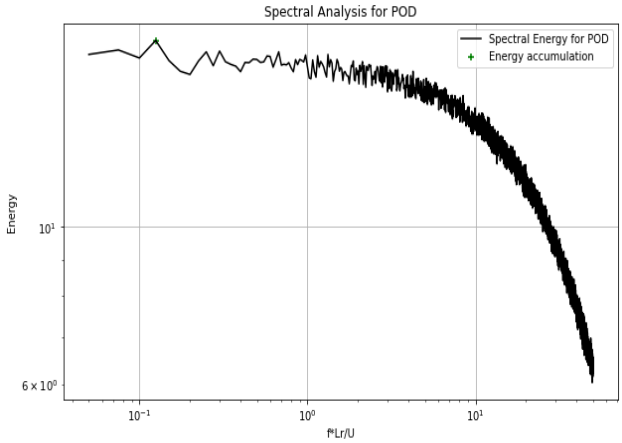

Fig. 17 Non-dimensional power spectra of fluctuating reduced order X Velocity (POD mode 1) measured at x/h=1.5 for our current study at Re_h = 89100

In mode 1 contour, we observed a distinct oscillation in the shear layer, which is clearly visible in Fig. 16. We observed a bulb that narrows and expands, with oscillations reaching a minimum negative value between x/h=1.8 and x/h=3.5. This dynamic is the most significant and important in the separated flow dynamics on BFS. Targeting control of this specific dynamic could yield valuable results, enhancing overall performance and reducing drag forces.

The quantification of this oscillation using spectral analysis revealed a frequency of approximately 5 oscillations per second. Remarkably, this observed frequency closely corresponds to the Strouhal number of 0.12, a frequency associated with flapping dynamics as reported in the existing literature. Consequently, our analysis suggests that the dominant dynamic behavior captured in POD mode 1, as shown in Fig. 17, is primarily representative of the flapping instability.

Figure 18 illustrates a machine learning model enhanced with (POD) for greater accuracy, designed to predict low order velocity using wall pressure data. Initially, wall pressure measurements and X velocity data are collected. The X velocity data undergoes POD, to reduce the dynamics dimensionality while preserving its most significant features. This step makes the data more manageable and improves the performance of the machine learning model. The reduced data and the wall pressure measurements are then used to train a (LSTM) (NN). Once trained, the model can predict the low order velocity using only the wall pressure points as input.

The training process resulted in a minimal loss of 5.35%, and the validation loss was 9.08% as shown in Fig. 19, which remains within acceptable limits.

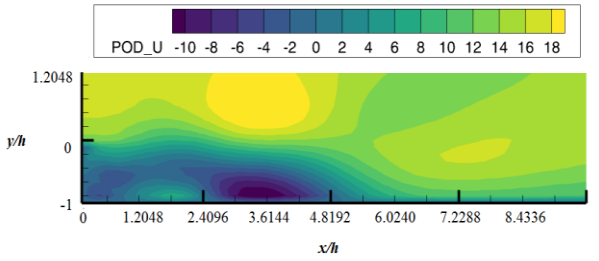

a) POD X velocity mode 1 at t_1.

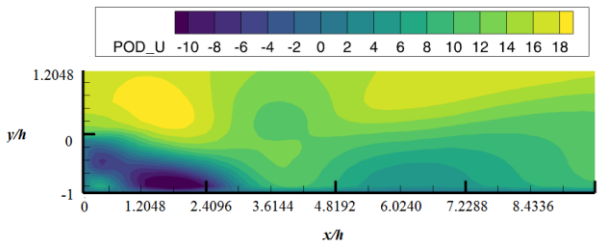

b) POD X velocity mode 1 at t_2.

Fig. 16 Contours at different instant of reduced order at mode 1 of X velocity

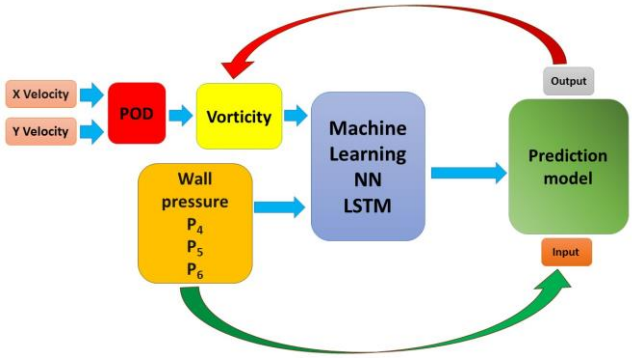

Fig. 18 Machine learning model with reduced order longitudinal velocity and ten wall pressure points

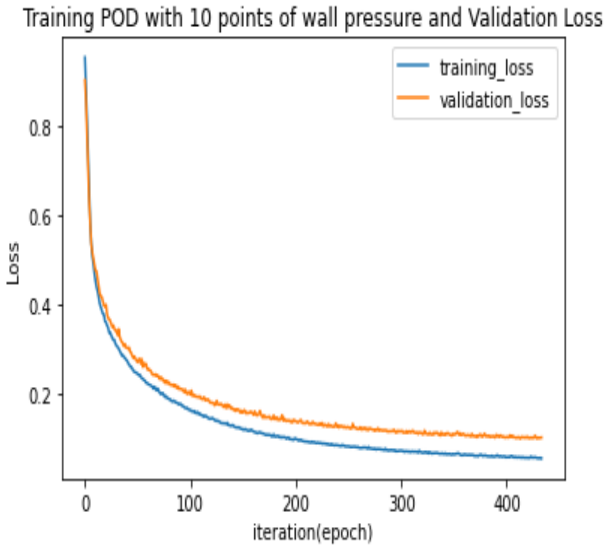

Fig. 19 Training pod with 10 points of wall pressure

Notably, the model exhibited accurate predictions, successfully preserving the correct topology of the reduced order of X velocity contours at different instants, as demonstrated in Fig. 20, the MSE is estimated to 5,064%. Also, specter analysis for predicted reduced order X velocity showed a good agreement with the original one (Fig. 21).

4.3 Study of the Best Region of Wall Pressure Measurement for Prediction

In this part, we use three points combinations of wall pressure that predict velocity with less mean squared error (MSE). We chose three points to see that the combination of different places (such as vertical and horizontal walls) of measurements is necessary to get maximum of information.

1. Dataset Preparation: Collect the dataset that includes wall pressure measurements and corresponding velocity values.

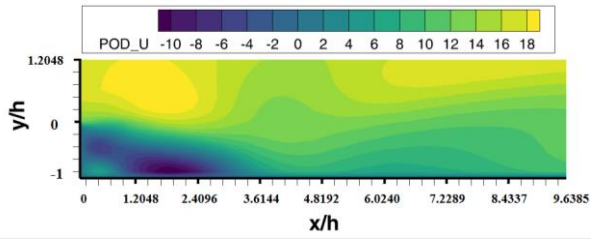

a) Original POD mode 1 at t_1

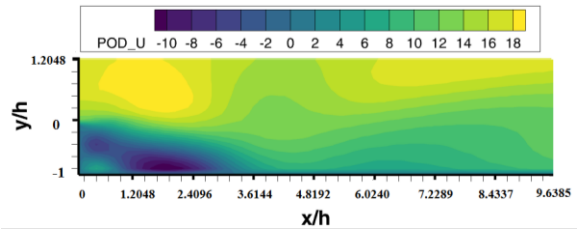

b) Predicted POD mode 1 at t_1

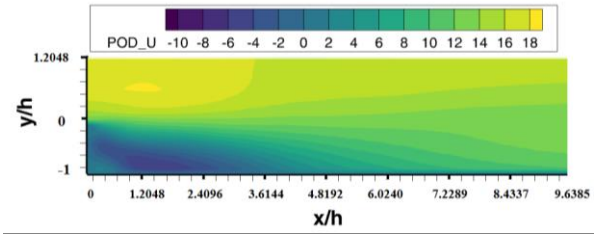

c) Original POD mode 1 at t_2

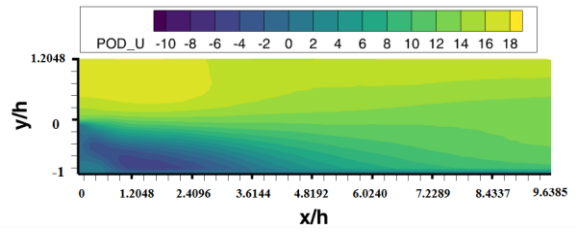

d) Predicted POD mode 1 at t_2

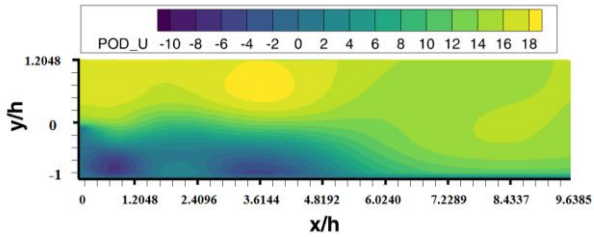

e) Original POD mode 1 at t_3

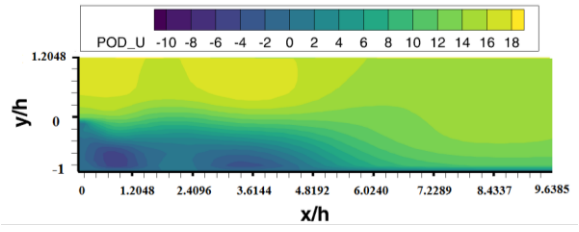

f) Predicted POD mode 1 at t_3

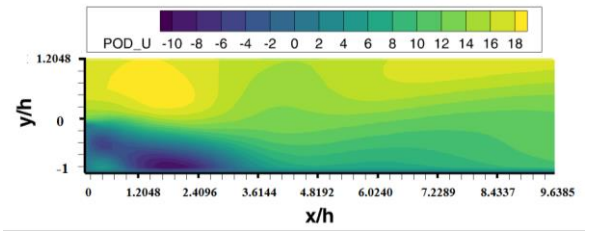

g) Original POD mode 1 at t_4

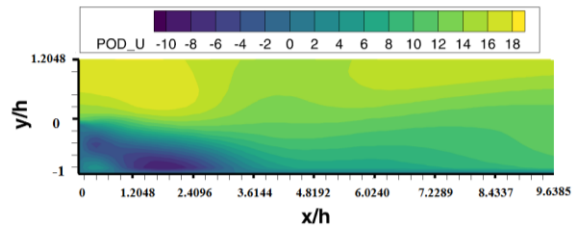

(h) Predicted POD mode 1 at t_4

Fig. 20 Predicting reduced order X velocity contours with ten points of wall pressure at different instants (t_1, t_2, t_3, t_4 stands for different instants of time flow)

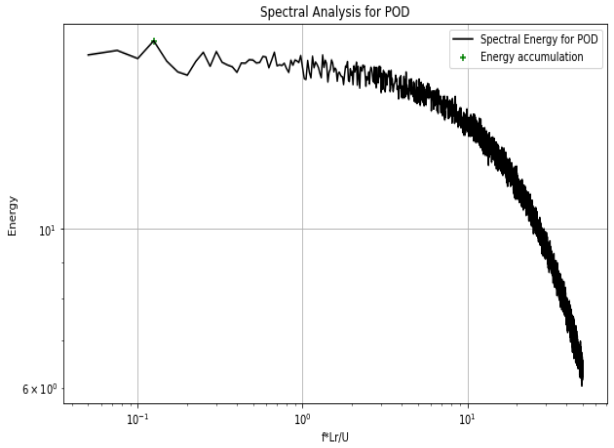

Fig. 21 Non-dimensional power spectra of fluctuating predicted reduced order X Velocity POD mode 1 with ten points of wall pressure at Re_h = 89100

2. Feature Selection: Select the three points (by combining three from the ten points defined before) for predicting velocity based on wall pressure.
3. Split the Dataset: Divide the dataset into training and testing sets. The training set will be used to train the prediction model. while the testing set will be used to evaluate its performance.
4. Model Training: Use a regression algorithm to train a model based on the selected three points (features) and the corresponding velocity values in the training set.
5. Model Evaluation: Evaluate the trained model's performance using the testing set. Calculate the (MSE) between the predicted velocity values and the actual velocity values in the testing set.
6. Iterate and Optimize: Repeat steps 2–5 with different combinations of three points to find the combination that yields the lowest MSE. using random search to explore different combinations efficiently.
7. Select the Best Combination: Compare the MSE values obtained for different combinations and select the one with the lowest MSE as the best combination of three points for predicting velocity based on wall pressure.
8. Validate the Model: Once selecting the best combination, and validate the model's performance by applying it.
9. By following these steps, you can systematically study the best three points combinations of wall pressure that tell us the best region to predict velocity with the least amount of error (MSE) and improve the accuracy of predictions.

Our comprehensive analysis has led us to a compelling conclusion: the points situated beneath the shear layer (4,5,6) as shown in Fig 22, emerge as the most favorable candidates for constructing combinations of three points that possess a remarkable capability to predict the true dynamics of the system. By focusing on these specific points, we are strategically targeting a region that exhibits a strong correlation with the underlying dynamic behavior. This region, characterized by its proximity to the shear layer, plays a pivotal role in shaping the flow patterns and influencing the overall system dynamics. The rationale behind selecting combinations of three points lies in the power of their collective information. Considering multiple points simultaneously, we can leverage the spatial relationships between them and capture a broader perspective of the system's behavior. Each point contributes valuable insights into the local flow characteristics, and when combined, they offer a comprehensive representation of the complex interactions occurring within the system. We have established that these three points combinations exhibit a significantly lower (MSE) compared to alternative approaches. This reduction in error signifies the enhanced predictive accuracy, enabling us to make more reliable predictions.

The spectral analysis was done on the predicted lower-order x velocity (Fig. 23), utilizing the three most

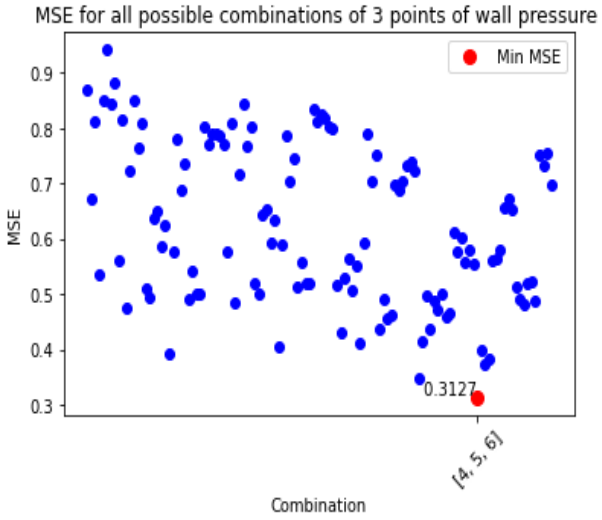

Fig. 22 MSE for all possible combinations of three points of wall pressure

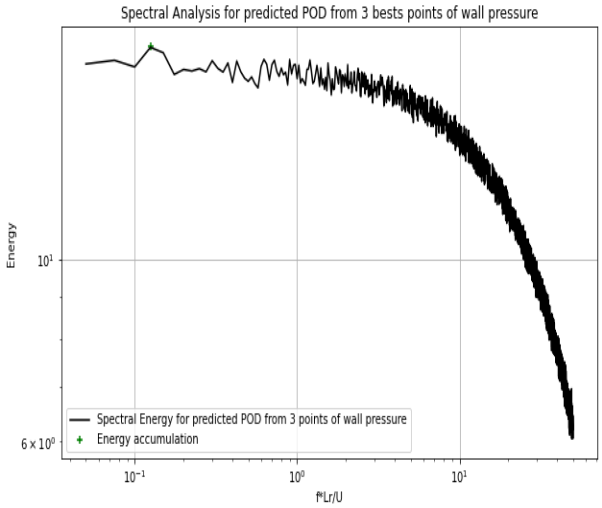

Fig. 23 Non-dimensional power spectra of fluctuating predicted reduced order X Velocity POD mode 1 using three best wall pressure points measured at x/h=1.5 at Re_h = 89100

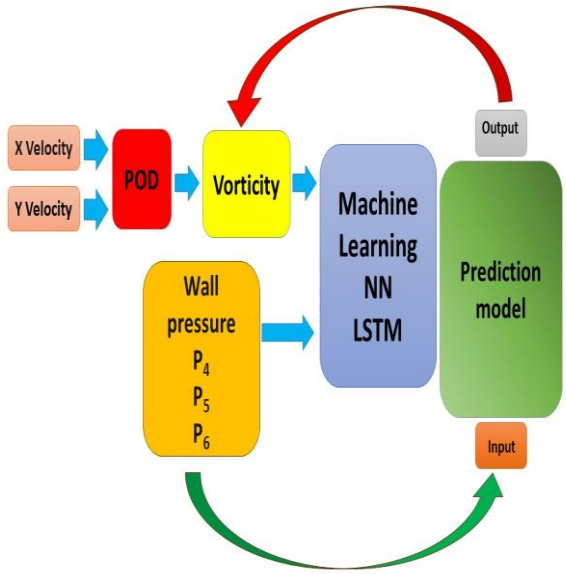

Fig. 24 Machine learning model with reduced order vorticity and best three wall pressure points

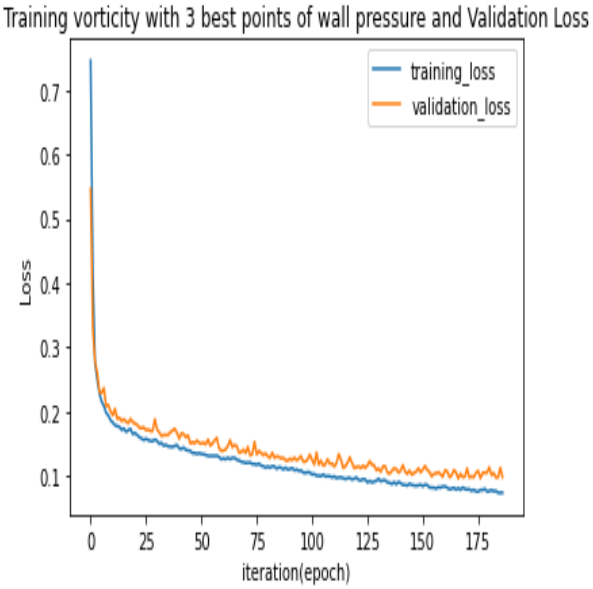

Fig. 25 Training reduced order vorticity magnitude with three best points of wall pressure

favorable wall pressure positions. It displayed a similar peak compared to the same analysis done on the original dynamics (Fig. 17) and the anticipated predicted dynamics using ten measurement points (Fig. 21). This peak represents the most significant dynamic in low frequencies, which is the flapping of shear layer and its prediction in real time is sufficient to establish flow control based on feedback information.

4.4 Training Reduced Order Vorticity with Wall Pressure

Vorticity is a vital concept as it depends on all velocity components, as shown in equation 6, and is closely linked to wall pressure. (As shown above, both longitudinal and normal velocity are in relation to wall pressure). This relationship makes it a valuable tool for machine learning and flow prediction. Also, shear layer regions are visible through vorticity contours, which offer the ability to effectively control the flow by knowing the position of shear layers.

$$\zeta = \nabla \times V = \left(\frac{\partial v}{\partial x}\right) - \left(\frac{\partial u}{\partial y}\right) \quad (6)$$

Figure 24 illustrates a machine learning model designed to predict low order vorticity using wall pressure data, with enhanced accuracy (POD). The process begins with the collection of X and Y velocity data, which undergoes POD to reduce dimensionality. This reduced data is then used to compute vorticity. Concurrently, wall pressure measurements at points P_4, P_5, and P_6 are collected. These inputs are fed into a (LSTM) (NN), which is trained using only three wall pressure points. This limited number of measurement points makes the approach particularly useful in practical scenarios where wall pressure sensors are restricted. Once trained, the prediction model can utilize the three wall pressure points to predict low order vorticity. This method is valuable for real time applications in flow control. The training phase resulted in a minimal loss of 7.33%, with a validation loss of 9.41% (presented in Fig. 25), both within acceptable limits. Importantly, the model demonstrated accurate predictions, maintaining the correct topology of reduced-order vorticity magnitude contours across various instances (see Fig. 26). The estimated MSE was 23.472%, attributed to the reduced correlation with pressure after partial derivation. This prediction was performed using only three points, indicating that increasing the number of data points could improve accuracy, but it does not impact the topology information.

After thoroughly analyzing the predictions of the low-order vorticity dataset across all time instants, we observed that the model consistently and accurately reflects the topology of the vortices. This includes not only the precise positioning of the vortices but also the accurate identification of maximum and minimum value locations. Additionally, the model demonstrated a strong capability in predicting the high vorticity values at the wall immediately after the (BFS), which signifies the reformation and strengthening of the new boundary layer. These accurate predictions are indicative of the model's robustness and reliability in capturing the critical aspects of separated flow dynamics. Consequently, we can confidently conclude that using just three wall pressure measurements is sufficient to provide comprehensive information about all the essential dynamics occurring over the BFS across all time instants. Although there is a slight difference between the original and predicted values in terms of scale, but the positions of the vortices are highly accurate. This minor discrepancy in value does not affect the overall topology information, which remains correct and reliable. As a result, this difference does not impact the essential data needed for effective feedback control in managing the flow dynamics.

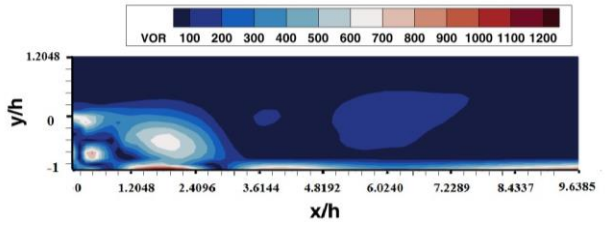

(a) Original reduced order vorticity at t_1

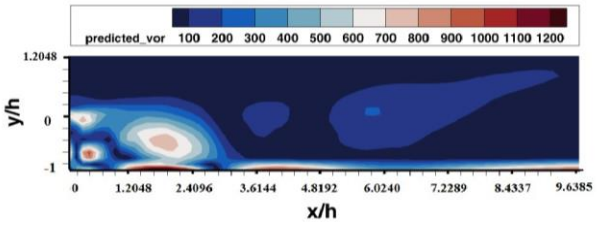

b) Predicted reduced order vorticity using three best wall pressure points at t_1

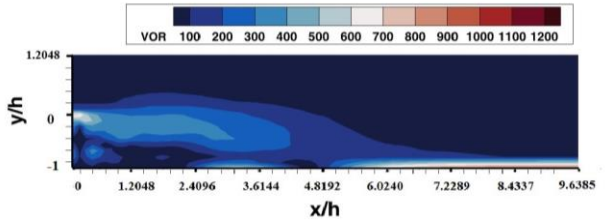

(c) Original reduced order vorticity at t_2

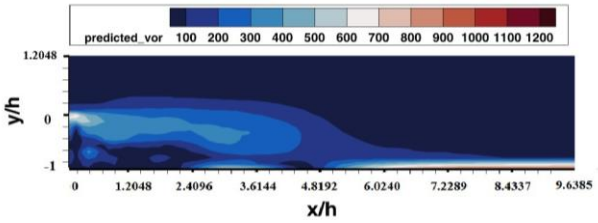

(d) Predicted reduced order vorticity using three best wall pressure points at t_2

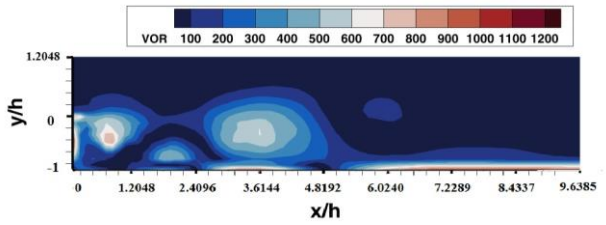

(e) Original reduced order vorticity at t_3.

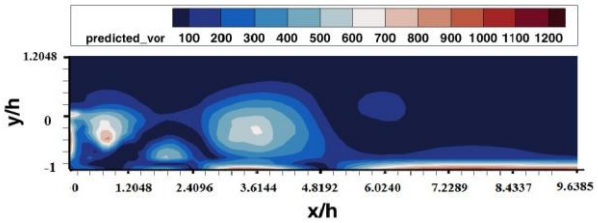

(f) Predicted reduced order vorticity using three best wall pressure points at t_3

Fig. 26 Prediction of low order vorticity magnitude using three best points wall pressure. ***(t_1, t_2, t_3 stands for different instants of time flow)***

CONCLUSION

This study highlights significant findings, on predicting separated flow dynamics within a high Reynolds number regime (Re_h = 89100), by utilizing artificial intelligence techniques, specifically the LSTM RNN method combined with (POD). The research emphasizes the effectiveness of the DES model in accurately replicating flow characteristics and wall pressure in such turbulent conditions, thereby establishing a reliable framework for analyzing such flow dynamics. In addition, spectral analysis is used to quantitatively evaluate flow characteristics, demonstrating strong alignment with experimental data and further enhancing confidence in the DES model's accuracy. Establishing a correlation between the velocity field and wall pressure is crucial before applying machine learning techniques. The study demonstrates that velocity fields have a strong relationship with wall pressure points around the recirculation zone. The integration of AI methods, particularly the LSTM RNN, facilitates the development of a deep learning framework that effectively links wall pressure points with the velocity field, yielding promising results in predicting flow dynamics. The research highlights the LSTM model's ability to make precise velocity magnitude predictions, achieving a low (MSE) of 13.48% when utilizing data from ten wall pressure points. The application of POD to reduce system dimensionality further enhances prediction accuracy, lowering the MSE to 5.07%. This approach not only retains essential dynamics but also improves computational efficiency and the learning process. Additionally, the study investigates different combinations of pressure measurements to determine the most effective region for velocity prediction. Remarkably, it demonstrates that even with only three wall pressure points, the model can achieve an acceptable MSE of 23.48% for low-order vorticity predictions. This finding is crucial for developing advanced control systems that require minimal data input, and establishing a closed-loop control system to manage separated flow on a (BFS). However, a noted limitation of this study is the significant computational resources required and the necessity for large datasets to enhance the model's robustness and reliability.

CONFLICT OF INTEREST

The author declares that there is no conflict of financial or non-financial interest to disclose.

AUTHORS CONTRIBUTION

S. Kouah: Data curation, Investigation, Software, Visualization, Formal analysis, Writing – original draft; **F. Fadla**: Data curation, Resources, Methodology, Writing – review & editing, Supervision; **M. Roudane**: Methodology, Supervision, review & editing.

REFERENCES

Almohammadi, K. M. (2020). Assessment of reattachment length using turbulence models on

backward facing step (BFS) for turbulent flow with modified general richardson method. *Arabian Journal for Science and Engineering*, *45*(11), 9293–9303. https://doi.org/10.1007/s13369-020-04695-0

Altché, F., & Fortelle, A. D. L. (2017). An LSTM network for highway trajectory prediction. In *Proceedings ofthe IEEE 20th International Conference on Intelligent Transportation Systems*. Piscataway, NJ: IEEE. https://doi.org/10.48550/arXiv.1801.07962

Antonio, V., & Lacerda De Brederode, S. (n.d.). *Three-dimensional effects in nominally two-dimensional flows*. https://api.semanticscholar.org/CorpusID:130177294

Bengio, Y. (2009). Learning deep Architectures for AI. *Foundations and Trends in Machine Learning*, *2*(1), 1–127. https://doi.org/10.1561/2200000006

Brown, B., Yu, X., & Garverick, S. (2004). Mixed-mode analog VLSI continuous-time recurrent neural network. In *Circuits, Signals, and Systems: IASTED International Conference Proceedings*. https://dblp.org/rec/conf/iastedCCS/BrownYG04

Carrio, A., Sampedro, C., Rodriguez-Ramos, A., & Campoy, P. (2017). A review of deep learning methods and applications for unmanned aerial Vehicles. *Journal of Sensors*, *2*, 1–13. https://doi.org/10.1155/2017/3296874

Chen, T. B., & Soo, V. W. (1996). A comparative study of recurrent neural network architectures on learning temporal sequences. In *Proceedings of the IEEE International Conference on Neural Networks. Piscataway*, NJ: IEEE. https://doi.org/10.1109/ICNN.1996.549199

Chovet, C., Lippert, M., Foucaut, J. M., & Keirsbulck, L. (2017). Dynamical aspects of a backward-facing step flow at large Reynolds numbers. *Experiments in Fluids*, *58*(11). https://doi.org/10.1007/s00348-017-2444-5

Chovet, C., Lippert, M., Keirsbulck, L., & Foucaut, J. M. (2019). Unsteady behavior of a backward-facing step in forced flow. *Flow, Turbulence and Combustion*, *102*(1), 145–165. https://doi.org/10.1007/s10494-018-9944-0

Duriez, T., Brunton, S. L., & Noack, B. R. (n.d.). *Fluid Mechanics and Its Applications Machine Learning Control-Taming Nonlinear Dynamics and Turbulence*. http://doi.org/10.1007/978-3-319-40624-4

Elman, J. L. (1990). Finding structure in time. *Cognitive Science*, *14*(2), 179–211. https://doi.org/10.1016/0364-0213(90)90002-E

Fadla, F., Alizard, F., Keirsbulck, L., Robinet, J. C., Laval, J. P., Foucaut, J. M., Chovet, C., Alizard, F., & Lippert, M. (2019). Science Arts & Métiers (SAM) investigation of the dynamics in separated turbulent flow. *European Journal of Mechanics-B/Fluids*, https://doi.org/10.1016/j.euromechflu.2019.01.006

Fadla, F., Graziani, A., Kerherve, F., Mathis, R., Lippert, M., Uystepruyst, D., & Keirsbulck, L. (2016). Electrochemical measurements for real-time stochastic reconstruction of large-scale dynamics of a separated flow. *Journal of Fluids Engineering, Transactions of the ASME*, *138*(12). https://doi.org/10.1115/1.4034198

Fernández, S., Graves, A., & Schmidhuber, J. (2007). An application of recurrent neural networks to discriminative keyword spotting. In *Proceedings of the International Conference on Artificial Neural Networks* (pp. 220–229). Berlin: Springer. https://doi.org/10.1007/978-3-540-74695-9_23

Fukushima, K. (1980). Neocognitron: A self-organizing neural network model for a mechanism of pattern recognition unaffected by shift in position. *Biological Cybernetics*, *36*(4), 193–202. https://doi.org/10.1007/BF00344251

Giannopoulos, A., & Aider, J. L. (2020). Prediction of the dynamics of a backward-facing step flow using focused time-delay neural networks and particle image velocimetry data-sets. *International Journal of Heat and Fluid Flow*, *82*. https://doi.org/10.1016/j.ijheatfluidflow.2019.108533

Gallagher, J. C., Boddhu, S. K., & Vigraham, S. (2005). A reconfigurable continuous time recurrent neural network for evolvable hardware applications. In *Proceedings of the 2005 IEEE Congress on Evolutionary Computation*. Piscataway, NJ: IEEE. http://doi.org/10.1109/EH.2005.5

Guo, Y., Liu, Y., Georgiou, T., & Lew, M. S. (2017). A review of semantic segmentation using deep neural networks. *International Journal of Multimedia Information Retrieval*, *2*, 1–7. https://doi.org/10.1007/s13735-017-0141-z

He, T., & Droppo, J. (2016). Exploiting LSTM structure in deep neural networks for speech recognition. In *Proceedings ofthe IEEE International Conference on Acoustics, Speech and Signal Processing* (pp. 5445–5449). Piscataway, NJ: IEEE. https://doi.org/10.1109/ICASSP.2016.7472718

Hsu, W. N., Zhang, Y., Lee, A., & Glass, J. (2016). Exploiting depth and highway connections in convolutional recurrent deep neural networks for speech recognition. *Cell*, *50*(1), 395–399. https://doi.org/10.21437/Interspeech.2016-515

Ivakhnenko, A. G., & Lapa, V. G. (1965). *Cybernetic predicting devices. Sacramento*, CA: CCM Information Corporation. https://api.semanticscholar.org/CorpusID:61108232

Ivakhnenko, A. G. (1971). Polynomial theory of complex systems. *IEEE Transactions on Systems, Man and Cybernetics*, *4*, 364–378. http://doi.org/10.1109/TSMC.1971.4308320

Jordan, M. (1986). Attractor dynamics and parallelism in a connectionist sequential machine. In *Proceedings of the Annual Conference of the Cognitive Science Society* (pp.531–546). Piscataway, NJ: IEEE. https://escholarship.org/uc/item/1fg2j76h

Khan, S., & Yairi, T. (2018). A review on the application of deep learning in system health management. *Mechanical Systems and Signal Processing*, *107*, 241-265. https://doi.org/10.1016/j.ymssp.2017.11.024

Kumar, K. R., & Selvaraj, M. (2023). Novel deep learning model for predicting wind velocity and power estimation in advanced INVELOX wind turbines. *Journal of Applied Fluid Mechanics*, *16*(6), 1256–1268. https://doi.org/10.47176/jafm.16.06.1637

LeCun, Y., Bottou, L., Bengio, Y., & Haffner, P. (1998). Gradient-based learning applied to document recognition. Proceedings of the IEEE, 86(11), 2278–2324. http://doi.org/10.1109/5.726791

Luo, D. (2019). Numerical simulation of turbulent flow over a backward facing step using partially averaged Navier-Stokes method. *Journal of Mechanical Science and Technology*, *33*(5), 2137–2148. https://doi.org/10.1007/s12206-019-0416-9

Mallinar, N., &Rosset, C. (2018). Deep canonically correlated LSTMs. https://doi.org/10.48550/arXiv.1801.05407

Mehrez, Z., Bouterra, M., Cafsi, A. El, Belghith, A., & Le Quéré, P. (2010). Simulation of the periodically perturbed separated and reattaching flow over a backward-facing step. *Journal of Applied Fluid Mechanics*, *3*(2). https://doi.org/10.36884/jafm.3.02.11883

Ötügen, M. V. (1991). Ex rimeas m l mds expansion ratio effects on the separated shear layer and reattachment downstream of a backward-facing step. *Experiments in Fluids*, 10.

Palangi, H., Deng, L., Shen, Y., Gao, J., He, X., Chen, J., & Ward, R. (2015). Deep sentence embedding using the long short-term memory network: Analysis and application to information retrieval. *IEEE/ACM Transactions on Audio Speech and Language Processing*, *24*(4), 694–707. https://doi.org/10.48550/arXiv.1502.06922

Probst, A., Radespiel, R., Wolf, C., Knopp, T., & Schwamborn, D. (2010). *A Comparison of Detached-Eddy Simulation and Reynolds-Stress Modelling Applied to the Flow over a Backward-Facing Step and an Airfoil at Stall*. https://doi.org/10.2514/6.2010-920

Pearlmutter, B. A. (1989). Learning state space trajectories in recurrent neural networks. *Neural Computation*, *1*(2), 263–269. https://doi.org/10.1162/neco.1989.1.2.263

Qu, Z., Haghani, P., Weinstein, E., & Moreno, P. (2017). Syllable-based acoustic modeling with CTC-SMBR-LSTM. In *Proceedings of the IEEE Automatic Speech Recognition and Understanding Workshop* (pp. 173–177). Piscataway, NJ: IEEE. https://doi.org/10.1109/ASRU.2017.8268932

Rajabi, E., & Kavianpour, M. R. (2012). Intelligent prediction of turbulent flow over backward-facing step using direct numerical simulation data. *Engineering Applications of Computational Fluid Mechanics*, *6*(4), 490–503. https://doi.org/10.1080/19942060.2012.11015437

Ranzato, M. A., Szlam, A., Bruna, J., Mathieu, M., Collobert, R., & Chopra, S. (2014). Video (language) modeling: A baseline for generative models of natural-videos. https://doi.org/10.48550/arXiv.1412.6604

Rawat, W., &Wang, Z. (2017). Deep convolutional neural Networks for image classification: A comprehensive review. *Neural Computation*, *29*(9), 1–10. https://doi.org/10.1162/NECO_a_00990

Robinson, A. J., & Fallside, F. (1987). The utility driven dynamic error propagation network. Cambridge: University of Cambridge Department of Engineering. https://www.researchgate.net/publication/243683010_The_utility_driven_dynamic_error_propagation_network

Sak, H. I., Senior, A., & Beaufays, F. O. (2014). Long short-term memory based recurrent neural network architectures for large vocabulary speech recognition. https://doi.org/10.48550/arXiv.1402.1128

Šarić, S., Jakirlić, S., & Tropea, C. (2005). A periodically perturbed backward-facing step flow by means of LES, des and T-RANS: An example of flow separation control. *Journal of Fluids Engineering, Transactions of the ASME*, *127*(5), 879–887. https://doi.org/10.1115/1.2012502

Sharma, P., & Singh, A. (2017). Era of deep neural networks: A review. In *Proceedings ofthe 8th International Conference on Computing, Communication and Networking Technologies* (pp. 1–5). Piscataway, NJ: IEEE. https://doi.org/10.1109/ICCCNT.2017.8203938

Singh, A. P., Medida, S., & Duraisamy, K. (2017). Machine-learning-augmented predictive modeling of turbulent separated flows over airfoils. *AIAA Journal*, *55*(7), 2215–2227. https://doi.org/10.2514/1.J055595

Smirnov, E. M., Smirnovsky, A. A., Schur, N. A., Zaitsev, D. K., & Smirnov, P. E. (2018). Comparison of RANS and IDDES solutions for turbulent flow and heat transfer past a backward-facing step. *Heat and Mass Transfer*, *54*(8), 2231–2241. https://doi.org/10.1007/s00231-017-2207-0

Sohankar, A., Khodadadi, M., Rangraz, E., & Alam, M. M. (2019). Control of flow and heat transfer over two inline square cylinders. *Physics of Fluids*, *31*(12). https://doi.org/10.1063/1.5128751

Šter, B. (2013). Selective recurrent neural network. *Neural Processing Letters*, *38*(1),1–15 https://doi.org/10.1007/s11063-012-9259-4

Sujar Garrido, P., Moreau, É., Bonnet, J.-P., Benard, N., & Éric Moreau, M. (2014). *Active control of the turbulent flow downstream of a backward facing step with dielectric barrier discharge plasma actuators* [Doctoral dissertation, Poitiers]. https://api.semanticscholar.org/CorpusID:92790265

Talele, V., Mathew, V. K., Sonawane, N., Sanap, S., Chandak, A., & Nema, A. (2021). CFD and ANN approach to predict the flow pattern around the square and rectangular bluff body for high Reynolds number. *Materials Today: Proceedings*, *47*, 3177–3185. https://doi.org/10.1016/j.matpr.2021.06.285

Werbos, P. J. (1988). Generalization of backpropagation with application to a recurrent gas market model. *Neural Networks*, *1*(4), 339–356. https://doi.org/10.1016/0893-6080(88)90007-X

Weng, J. J., Ahuja, N., & Huang, T. S. (1993, May). Learning recognition and segmentation of 3D objects from 2D images. In *Proceedings of the Fourth International Conference on Computer Vision* (pp. 121–128). Piscataway, NJ: IEEE. https://doi.org/10.1109/iccv.1993.378228

Williams, R. J. (1989). *Complexity of exact gradient computation algorithms for recurrent neural networks* (Technical Report NU-CCS-89-27). Boston: Northeastern University, College of Computer Science. https://modeldb.science/citations/107088

Yu, Y., Si, X., Hu, C., & Zhang, J. (2019). A review of recurrent neural networks: LSTM cells and network architectures. Neural computation, 31(7), 1235-1270. https://doi.org/10.1162/neco_a_01199